Biochimica et Biophysica Acta, 502 (1978) 1—10

BBA 47462

THE ORIENTATION OF A HEME OF CYTOCHROME *c* OXIDASE IN SUBMITOCHONDRIAL PARTICLES

HAYWOOD BLUM, H.J. HARMON *, J.S. LEIGH, J.C. SALERNO and BRITTON CHANCE

Johnson Research Foundation, Department of Biochemistry and Biophysics, School of Medicine, University of Pennsylvania, Philadelphia, Pa. 19104 (U.S.A.)

(Received September 16th, 1977)

Summary

The electron paramagnetic resonance of the low spin signal from oxidized cytochrome *c* oxidase has been studied in oreinted multilayers of submitochondrial and electron transport particles. Measurements of the angular variation of the EPR spectra with the multilayer plane orientation allow the determination of the heme orientation in the multilayer. The heme normal lies in the membrane plane and the *y*-axis of the heme makes an angle of 30° with the membrane normal. Analysis of the line shape reveals the presence of mosaic spread in the multilayer almost half of which is attributable to deviations of protein orientation within the membrane.

Introduction

Although cytochrome *c* oxidase contains two hemes (cytochrome *a* and a_3) and two copper atoms, the EPR signals of the fully oxidized enzyme reveal only a single heme and one copper atom [1]. The low spin heme EPR signal which is observed in the fully oxidized enzyme has been assigned to cytochrome *a* and a_3 or to both [2—6]. At the present time, most workers ascribe the signal to cytochrome a_3 [7].

Recent work using oriented multilayers made by centrifugation and partial drying of purified cytochrome oxidase vesicles [8], electron transport particles [9], and whole mitochondria [10] has shown that the heme planes are fixed relative to the membrane normal. In this report we present more detailed experimental results on oriented multilayers of cytochrome *c* oxidase electron transport particles and submitochondrial particles ** which allow us to

* Present address: School of Biological Sciences, Oklahoma State University, Stillwater, Okla. 74074, U.S.A.

** For the sake of clarity and historical definition, the term 'electron transport particle' is reserved in this communication for the particles prepared by the original alkaline treatment [11] and 'submitochondrial particles' for the cytochrome *c*-depleted sonicated preparations.

determine the spatial orientation of the observed heme. Through the application of a computer simulation program, we are able to explain the EPR line shapes and positions in detail and to assess the quality of the multilayers.

Methods

Sample preparation. Electron transport particles were prepared by the alkaline method of Crane et al. [11] from beef heart mitochondria and frozen in 0.25 M sucrose at −20°C until use. The sidedness of the electron transport particles was determined from the effect of the addition of protamine sulfate and exogenous cytochrome *c* on the rate of oxygen uptake at 25°C [12,13]. Previous experience indicates that the orientation of the particles remains inverted for periods up to 1 year in the frozen state. Frozen particles were thawed, homogenized, and diluted 15-fold with 5 mM Tris · HCl buffer (pH 7.4) prior to sedimentation at 78 000 × *g* for 30 min. The homogenized particles were again washed in Tris buffer. Following the second wash, the particles (approx. 20 mg) were suspended in 5 mM Tris · HCl and centrifuged at 78 000 × *g* for 30 min onto a sheet of mylar at the base of a cylindrical holder placed in a swinging-bucket centrifuge tube. The mylar sheet had previously been washed with detergent and water and then coated with a film of collodion by dipping in a 1% (v/v) ether/ethanol solution. After centrifugation, the multilayer pellet was placed in a 90% relative humidity atmosphere for at least 24 h. Such multilayers are stable in this environment for up to 5 days at 5°C and can be stored frozen for longer periods, as determined by the quality of the EPR orientation.

Submitochondrial particles depleted of cytochrome *c* were prepared from beef heart mitochondria already depleted of over 90% of their endogenous cytochrome *c* [14]. These mitochondria were suspended in 0.25 M sucrose/0.15 M KCl medium and washed twice by centrifuging at 24 000 × *g* for 15 min. The cytochrome *c*-depleted mitochondrial membranes were then sonicated in 0.25 M sucrose at full power in a Branson sonicator for two 3-min intervals in an ice-salt bath, with a 5 min cooling interval between sonications. The pH of the mitochondrial mixture did not change during the sonication. The sonicate was then centrifuged at 22 000 × *g* for 7 min (pellet discarded) three times to separate the light submitocondrial particles from the heavier mitochondrial fragments. The submitochondrial particles were then pelleted at 78 000 × *g* for 30 min and then washed and centrifuged onto mylar as described for electron transport particles.

Cytochrome content was determined from the reduced minus oxidized difference spectra obtained with a Cary 15 spectrophotometer. Particles (0.4 ml) were clarified with 0.1 ml 10% (w/v) potassium deoxycholate (pH 8.0). This clarified mixture was then diluted to 2.0 ml with 0.25 M sucrose/30 mM Tris · HCl (pH 7.4) buffer. The contents of the sample cuvette were reduced with dithionite and those of the reference cuvette oxidized with ferricyanide.

EPR. The hydrated multilayer on its mylar substrate was sliced into a rectangle approx. 5 × 10 mm and slipped into a plexiglas cuvette with interior dimensions 2 × 6 × 45 mm. The cuvette was mounted in a tubular holder/rotator and the entire assembly was inserted into a special large bore quartz

dewar in an Air Products LTD-3-110 flowing helium cryostat. The angular position of the rotator could be easily adjusted and reset to ±3°C, even at low temperatures (5—50K). The temperature was measured with calibrated carbon resistors placed directly below the sample holder in the helium gas path and set to 14K. The temperature difference between the sample and the resistor was less than 2 degrees. The temperature was continuously monitored and kept constant to ±0.5K during a complete angular run. The signal amplitude at 0° field angle (defined below) was monitored from time to time during a run in order to make sure that the spectrometer sensitivity was not drifting in time.

All EPR spectra were taken on a Varian E-4 EPR spectrometer with 100 kHz field modulation and equpped with a Varian E-231 TE102 rectangular cavity. Microwave power incident at the cavity was 5 mW nominal. The modulation amplitude was 10 G (1 mT). The microwave frequency was 9.2 GHz.

Results

The orientation of the applied magnetic field, H_0, to the membrane normal is shown in Fig. 1. In Fig. 2, the 0° orientation is for H_0 parallel to the membrane plane and 90° is for H_0 perpendicular to the membrane plane.

The signals shown in Fig. 2 are similar, with some exceptions, to the unoriented EPR spectrum of oxidized cytochrome *c* oxidase [2,15], a low-spin heme with principal *g* values of 3.0, 2.25, and 1.46. The signals near $g = 2.5$ in Fig. 2 are partly due to a minor component low-spin signal found in oxidized cytochrome *c* oxidase [15] and partly to a signal from the sample holder. The signals near $g = 2$ are ascribed to copper and oxidized iron-sulfur proteins which are not considered in this report.

The main feature noted in the $g = 3.0$ signal is that the shape is absorption-like but with a rather long tail on the high field side. Its intensity falls mono-

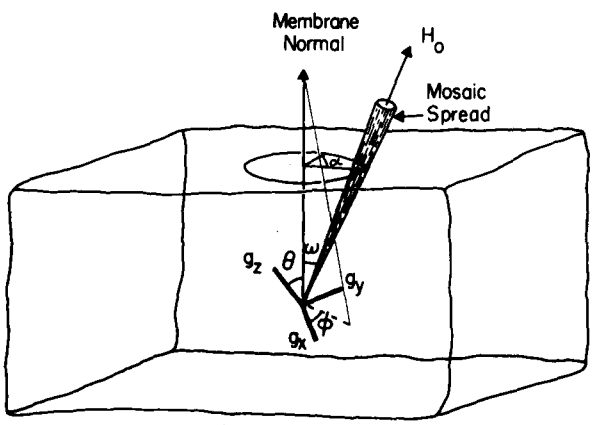

Fig. 1. Sketch of a general paramagnetic center with rhombic symmetry within an oriented membrane segment. θ and ϕ define the orientation of the principal *g* axes to the membrane normal. ω and α give the direction of the applied magnetic field, H_0, with respect to the membrane normal. As ω is varied from 0° to 90°, the field goes from perpendicular to the membrane plane to parallel to the membrane plane. To conform to earlier usage, however, we use the angle between the parallel to the membrane plane and H_0; that is, the complement of ω, to describe the orientation.

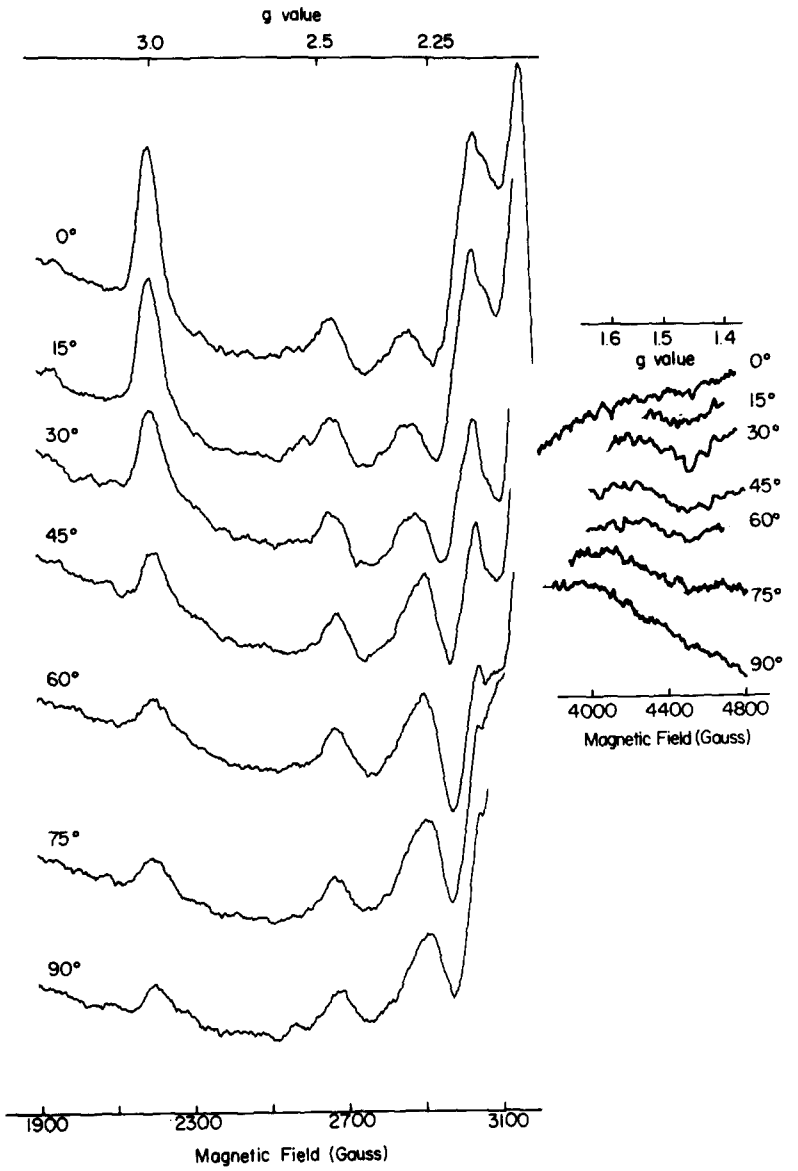

Fig. 2. EPR signals from oxidized cytochrome *c* oxidase for angles between the magnetic field and the multilayer plane from 0° to 90°. Left, in the region between $g = 2$ and $g = 3$; right, for the region near $g = 1.5$.

tonically with increasing angle. The $g = 2.25$ signal has a derivative shape. Its intensity is minimum at 0°, grows to a maximum at 60° and falls for field angles greater than 60°. The $g = 1.46$ signal is much weaker due to its large width. It has a maximum intensity at 30° and can scarcely be seen at all at other angles.

We have plotted the heights of the $g = 3.0$ and $g = 2.25$ signals in Fig. 3. The data points are shown as open circles or squares, normalized to the height of the $g = 3.0$ signal at 0°. Here we see more clearly that the $g = 2.25$ signal has a

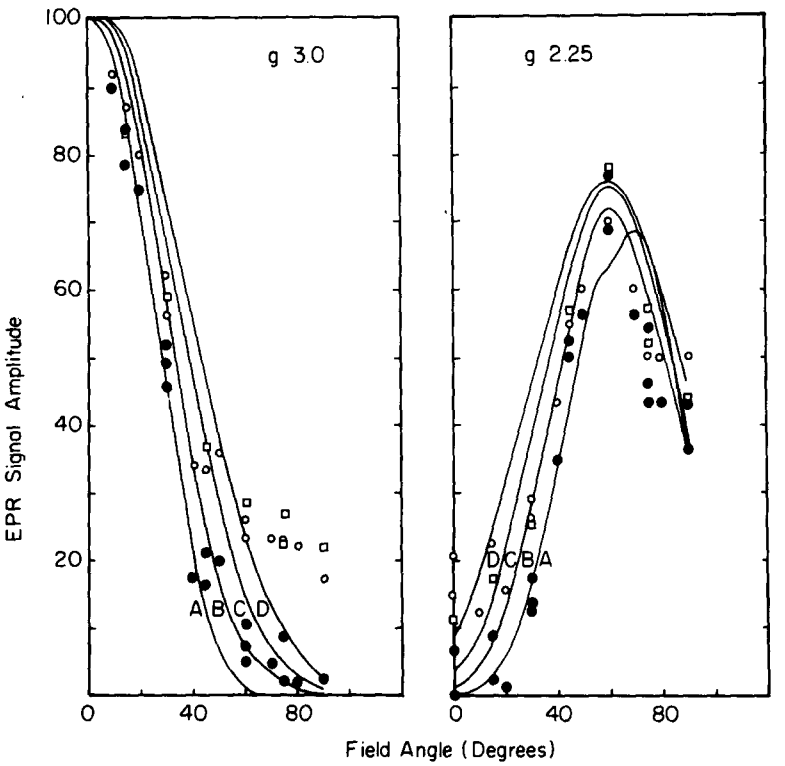

Fig. 3. Height of the EPR signal at (a) $g = 3.0$ (base to peak) and (b) $g = 2.25$ (peak to peak) plotted against field angle, normalized to the $g = 3.0$ signal at 0°. Open circle data points are electron transport particles (with cytochrome *c*); open squares are submitochondrial particles (cytochrome *c* depleted). Data corrected as described in the text for unoriented material are larger filled-in circles. Relative heights of $g = 3.0$ and $g = 2.25$ signals calculated from computer simulations, solid curves. Assumed Gaussian mosaic spread: A, 20°; B, 25°; C, 30°; D, 35°.

maximum amplitude at 60°, and its height is approx. 75% of the height of the $g = 3.0$ signal.

Except for the variation of amplitude with field angle, the experimental EPR spectra are almost powder-like. These results can be interpreted when the disorientation present in the membrane multilayer is taken into consideration. The disorientation or mosaic spread of the membrane, shown as a cone of angles in Fig. 1, has been estimated by X-ray diffraction. The mosaic spread tends to increase with multilayer thickness. It is modeled as having a Gaussian distribution of the tilts of the normals to the multilayer plane with half-width at half maximum of from 5° to 8° for thicker layers [16] of good model membranes. Our multilayers are somewhat thicker than those used as X-ray specimens.

This mosaic spread measurement comes from those well-stacked multilayer segments which can give an X-ray diffraction pattern. Unoriented material which cannot be seen by that method will nevertheless contribute to the EPR signals. This is discussed below.

We have analyzed the data presented above with the assistance of a computer simulation program. Given the principal *g* values, three line width parameters,

the mosaic spread, and the center orientation, a simulation of the EPR spectrum is computed. Referring to Fig. 1, we see that the angles θ and ϕ must be specified. Even for a perfect multilayer, with little or no mosaic spread, there is no order within the plane of the multilayer. The stimulation program must therefore average over the angle α, the angle ω (and its complement) remaining fixed by the experimental conditions. The simulation program will be described in detail elsewhere.

Fig. 4a shows a family of simulated spectra taken with varying field angle ω, assuming Gaussian derivative line shapes and only 1° of mosaic spread. We have taken $g_x = 1.5$, $g_y = 2.2$, and $g_z = 3.0$ as the principal values for the rhombic g tensor for cytochrome c oxidase [7] in the simulations. The simulation for 1° mosaic spread clearly does not fit the experimental data. The positions of the lines vary with angle rather than staying essentially at the principal g values. All the lines have the derivative-like character characteristic of single crystal spectra. The relative intensities of the lines do not fit the data.

We introduce mosaic spread by weighting the probability, W, for membrane orientation away from the specified angle as $W = W_0 \exp(-\ln 2 \cdot \Delta\omega^2/\Omega^2)$, where $\Delta\omega = \omega' - \omega$, ω' being the actual orientation angle, and Ω is the Gaussian mosaic spread parameter (half-width at half maximum). Ω is related to the standard deviation σ by $\sigma = (2\ln 2)^{-1/2} \cdot \Omega = 0.849\Omega$. We then average over all possible angles ω' and α.

If Ω is large enough, as in Fig. 5 where it is equal to 1000°, a powder pattern is generated. In this case all orientations are essentially equally likely. This simulation compares favorably with published spectra [15].

Fig. 4b shows the simulated spectra for various field angles when the mosaic spread is 25°. θ and ϕ have been chosen as 90° and 60°, respectively, and the line width parameters are unchanged from Fig. 4a. In this case we note that the introduction of mosaic spread causes the principal g values to be emphasized so that the line positions are unchanging. The $g = 3.0$ and $g = 1.5$ lines have absorption-like shapes and the $g = 3.0$ line tends to have a broad high field tail. The $g = 3.0$ signal is maximal at 0° falling to zero at 90°. The $g = 2.2$ signal has its maximum amplitude at 60°, whereas the $g = 1.5$ signal is largest at 30°.

The choice of heme angles, $\theta = 90°$ and $\phi = 60°$; that is, the z-axis of the heme lying in the multilayer plane ($\theta = 90°$), and the y-axis 30° from the multilayer normal ($\phi = 60°$) are dictated by the data. Choices of θ other than 90° cause the $g = 3.0$ signal to have a maximum at other than 0° field angles in contradiction to the data. Similarly, choices of ϕ away from 60° cause the $g = 2.2$ signal to peak at field angles other than 60°.

In Fig. 3 the heights of the $g = 3.0$ and $g = 2.2$ signals relative to the amplitude of the $g = 3.0$ signal at 0° are plotted for assumed mosaic spreads from 20° to 35° (solid curves). Although the general shape fits the data (open symbols), there are discrepancies for the $g = 3.0$ data at larger field angles and for the $g = 2.2$ data at smaller field angles.

Our multilayers are formed from particles of small diameter and we expected some end corrections. That is, as the vesicles become flattened to form multilayers, the ends may curve around. Larger vesicles will have relatively more area in the multilayer form than smaller vesicles but in every case a minor component must be substantially unoriented. An estimate of the unoriented

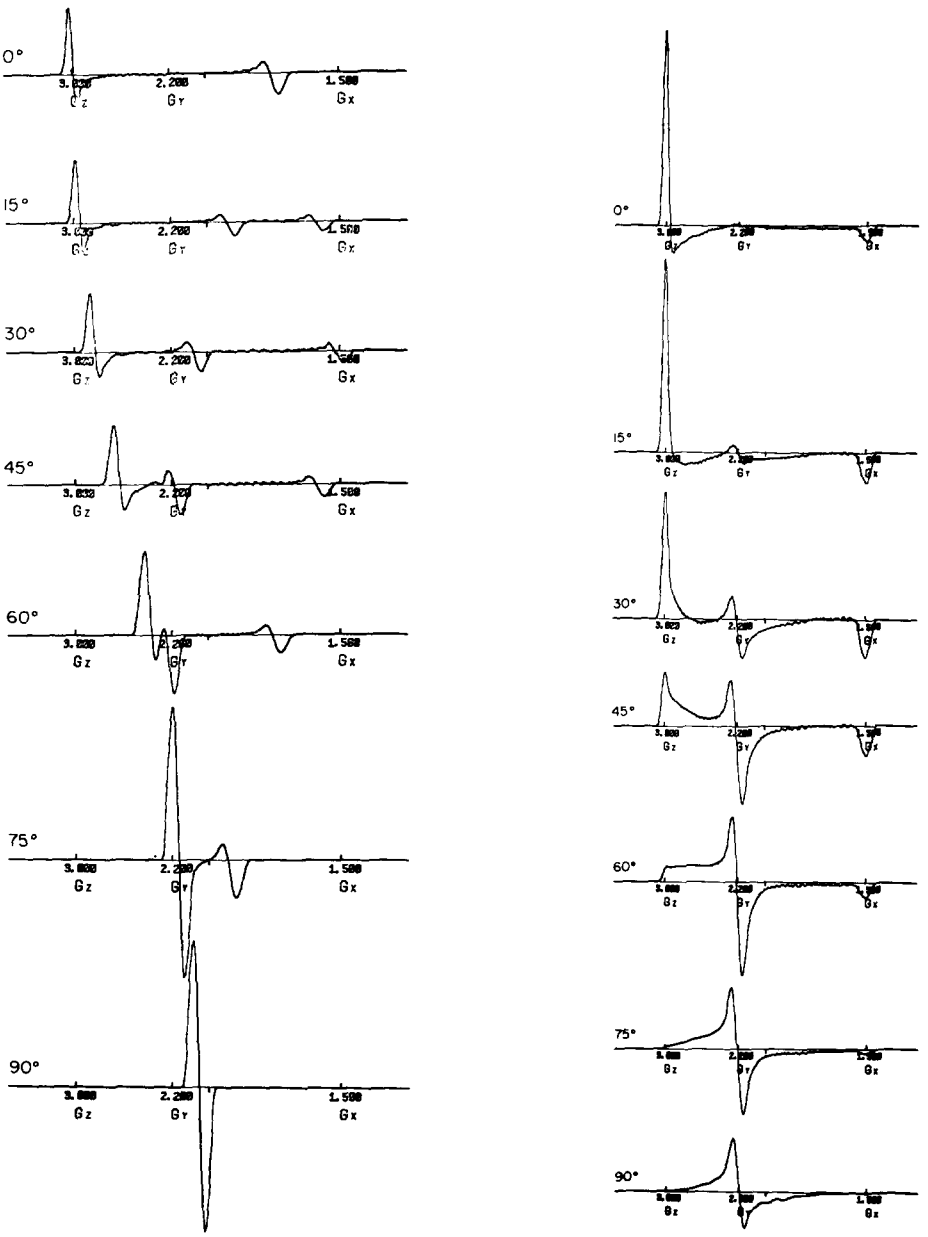

Fig. 4. Computer simulation of cytochrome *c* oxidase absorption derivative EPR spectrum versus angle of field relative to membrane plane. Center orientation defined in Fig. 1; $\theta = 90°, \phi = 60°$. The assumed line-widths (half-width at half maximum) were varied according to the expression $\Delta H^2 = \Delta H_x^2 \sin^2\theta_1 \cos^2\phi_1 + \Delta H_y^2 \sin^2\phi_1 + \Delta H_z^2 \cos^2\theta_1$, where θ_1 and ϕ_1 are the spherical angles between H_0 and the oxidase principal axes and ΔH_x, ΔH_y, ΔH_z are the three line-width parameters. The line-width spread is usually ascribe to '*g*-strain'; that is, a multitude of slightly different protein conformations causing line broadening through variations of the crystal field potentials which varies with *g* value [17,18]. Assumed line shape is Gaussian with half-width parameters: $\Delta H_x = 75$ G, $\Delta H_y = 50$ G, $\Delta H_z = 30$ G. Assumed Gaussian mosaic spread: (A) 1°; (B) 25°. Horizontal axis is linear in magnetic field with $g_x = 1.5$, $g_y = 2.2$, $g_z = 3.0$ indicated. $g = 2.0$ is also indicated.

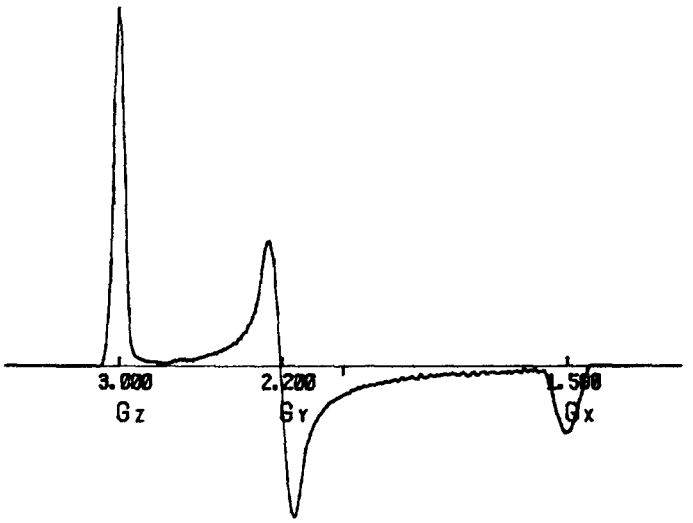

Fig. 5. Computer simulation as in Fig. 4. Powder pattern generated with mosaic spread of 1000°.

fraction can be made. If we take the surface area of a vesicle of radius R to be $4\pi R^2$, the curved portion of the surface on flattening will be approx. $2\pi R \cdot \pi r$, where r is the membrane thickness. This gives an unoriented fraction of $(\pi/2)(r/R)$, around 15% for 1000 Å diameter vesicles.

If we assume that 20% of the EPR signal comes from unoriented oxidase, we can subtract the powder pattern (Fig. 5) signals from the data in Fig. 3. If we then renormalize to the $g = 3.0$ peak at 0°, we get the solid circles plotted in Fig. 3. This data fits the 25° mosaic spread curve quite well (curve B of Fig. 3).

The mosaic spread of the EPR signals is thus approx. 10—15° greater than that of similar multilayers determined by X-ray diffraction [16]. This difference can be taken as the limit of the disorientation of the heme with respect to the membrane. Since the deviation of the sum of two Gaussian distributions is equal to the sum of the individual deviations [21], the spread in the chromophore orientation in the protein plus the spread in the protein orientation in the membrane adds up to 10—15°. Analyses of the EPR spectra in single crystals of ferricytochrome *c* [17] and hemoglobin and hemoglobin azide [18] indicate that the line-width arises mainly from three sources: an isotropic component, misorientation of the heme in the protein or the protein in the single crystal, and variations in the ligand field parameters from molecule to molecule. The estimated misorientation component had an root mean square deviation of 1.5° [17] to 2° [18] (half-widths of 1.8° to 2.2°). If we ascribe this entirely to misorientation of the heme within the molecule (which is certainly an overestimate due to the 'softness' of the crystals) and assume similar properties for cytochrome *c* oxidase, then the bulk (8—12°) of the mosaic spread is attributable to molecular misorientation within the membrane; that is, the heme is 'locked' in place securely in the protein. This argument, however, ignores the possibility of increased molecular conformational variability, suppressed in the crystal, contributing to the line width.

The Gaussian mosaic spread determined by optical polarization measurement

in the model system of membranous cytochrome oxidase [16] was 8—17° (half-width at half maximum).

Discussion

At this time our knowledge of the relationship between the principal g axes and the orientation of the porphyrin rests mainly on the EPR results of Mailer and Taylor [17] and the X-ray structure reported by Dickerson et al. [22] for horse heart cytochrome c. Their results are that the g_z axis lies within 5° of the heme normal whereas the g_x and g_y axes lie in the heme plane pointing toward the N-Fe-N directions in the heme ring. In the heme proteins metmyoglobin azide [20,23,24] and myoglobin cyanide [23,24] the g_z is 9° and 13°, respectively, from the heme normal and the g_x and g_y axes are approx. 45° from the N-Fe-N directions.

These measurements have been summarized by Taylor [26] who has also reviewed the theoretical calculations of the energy levels and g values of low-spin heme complexes. His conclusion is that g_y indicates the direction in the heme plane associated with the greatest unpaired spin density. In view of the Heme A structure, we can apply this result by suggesting that the g_y axis points toward the two nitrogen atoms whose pyrrole rings have the electron-withdrawing vinyl and formyl groups attached. Such a hypothetical model is presented in Fig. 6.

We have shown that the g_z direction for the heme of oxidized cytochrome c oxidase points parallel to the membrane plane confirming preliminary results [9] and work on whole mitochondria [10] and model systems [16]. To within our experimental accuracy, ±3%, we have found that the g_x axis is 30° and the g_y axis is 60°, respectively, from the multilayer plane.

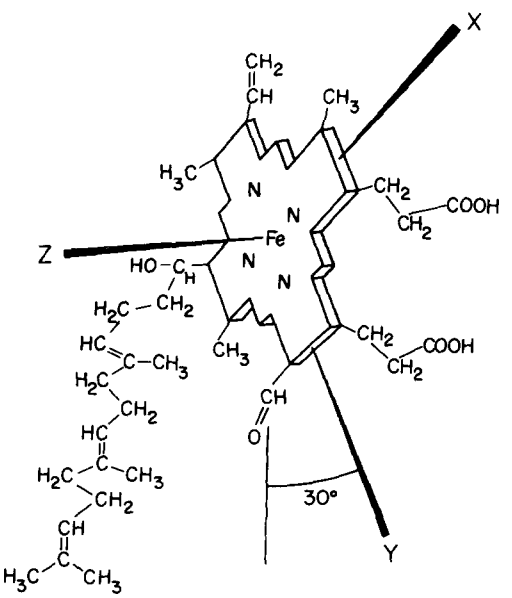

Fig. 6. Hypothetical cytochrome c oxidase heme orientation with respect to the membrane.

Acknowledgements

This work was supported by United States Public Health Grants GM 12202 and HL-15061-0551 and National Science Foundation Grant BMS 7513459.

References

1 Hartzell, C.R. and Beinert, H. (1974) Biochim. Biophys. Acta 368, 318—338
2 van Gelder, B.F. and Beinert, H. (1969) Biochim. Biophys. Acta 189, 1—24
3 Wilson, D.F. and Leigh, J.S. (1972) Arch. Biochem. Biophys. 150, 154—163
4 Tiesjema, R.H., Muijsers, A.O. and van Gelder, B.F. (1973) Biochim. Biophys. Acta 305, 19—28
5 Hartzell, C.R., Hansen, R.E. and Beinert, H. (1973) Proc. Natl. Acad. Sci. U.S. 70, 2477—2481
6 Wikstrom, M.K.F., Harmon, H.J., Ingledew, W.J. and Chance, B. (1976) FEBS Lett. 65, 259—277
7 Hartzell, C.R. and Beinert, H. (1976) Biochim. Biophys. Acta 423, 323—338
8 Blasie, J.K., Erecinska, M., Leigh, J.S. and Samuels, S. (1977) Biophys. J. 17, 63a
9 Leigh, J.S. and Harmon, H.J. (1977) Biophys. J. 17, 251a
10 Erecinska, M., Blasie, J.K. and Wilson, D.F. (1977) FEBS Lett. 76, 235—239
11 Crane, F.L., Glenn, J.L. and Green, D.E. (1956) Biochim. Biophys. Acta 22, 475—487
12 Harmon, H.J. and Crane, F.L. (1976) Biochim. Biophys. Acta 440, 45—48
13 Harmon, H.J., Hall, J.D. and Crane, F.L. (1974) Biochim. Biophys. Acta 344, 119—156
14 Harmon, H.J. and Crane, F.L. (1974) Biochem. Biophys. Res. Commun. 59, 326—333
15 Hartzell, C.R. and Beinert, H. (1974) Biochim. Biophys. Acta 368, 318—338
16 Blasie, J.K., Erecinska, M., Samuels, S. and Leigh, J.S. (1977) Biochim. Biophys. Acta 501, 33—52
17 Mailer, C. and Taylor, C.P.S. (1972) Can. J. Biochem. 50, 1048—1055
18 Eisenberger, R. and Pershan, P.S. (1967) J. Chem. Phys. 47, 3327—3333
19 Slade, E.F. and Ingram, D.J.E. (1968) Nature 220, 785
20 Helke, G.A., Ingram, D.J.E. and Slade, E.F. (1968) Proc. R. Soc. Lond. Ser. B 169, 275—288
21 Coffman, R.E. (1975) J. Chem. Phys. 79, 1129—1138
22 Dickerson, R.E., Takano, T., Eisenberg, D., Kallai, O.B., Samson, L. Cooper, A. and Margoliash, E. (1971) J. Biol. Chem. 246, 1511—1535
23 Gibson, J.F. and Ingram, D.J. (1957) Nature 180, 29—30
24 Hori, H. (1971) Biochim. Biophys. Acta 251, 227—235
25 Peisach, J., Blumberg, W.E. and Wyluda, B.J. (1971) Proc. 1st Eur. Biophys. Congr., 109—112
26 Taylor, C.P.S. (1977) Biochim. Biophys. Acta 491, 137—149